Shape, size, strain and correlations in quantum dot systems studied by grazing incidence X-ray scattering methods

T.H. Metzger[a,*], I. Kegel[a], R. Paniago[a,1], A. Lorke[a], J. Peisl[a], J. Schulze[b], I. Eisele[b], P. Schittenhelm[c], G. Abstreiter[c]

[a]Sektion Physik, Universität München, D80539 München, Germany
[b]Fakultät für Physik, Universität der Bundeswehr München, D85577 Neubiberg, Germany
[c]Walter Schottky Institut, Technische Univerität München, D85748 Garching, Germany

Abstract

We present results obtained by grazing incidence X-ray scattering methods on three different semiconductor heterostructures containing 3D islands ('quantum dots'). We show that the combination of the depth sensitivity of these methods and the use of synchrotron radiation allows for a full structural characterisation of the quantum dots. All samples systems were grown by molecular beam epitaxy. (1) Ge (15 nm) deposited on boron terminated Si(111) surfaces is shown to form relaxed triangular Ge pyramids with no orientational dispersion. We demonstrate how the 3-fold symmetry is obtained. (2) In the case of coherent InAs islands grown on GaAs(100), grazing incidence diffraction between the (220) surface reflections of InAs and GaAs reveals that the quantum dots are pseudmorphically strained at the interface to the substrate while they become fully relaxed at the top of the islands. In a novel approach ('iso-strain scattering') we are able to determine the interdependence of radius and strain in the dots which turns out to be linear. (3) In the third example of coherent Ge islands embedded in a Si/Ge superlattice we find correlations both laterally and in the growth direction. On the surface the dots are organised in a short range order square lattice. By increasing the scattering depth to investigate the superlattice, we find the buried Ge dots to be strongly correlated in the growth direction. Surface sensitive X-ray techniques using grazing incidence and exit angles have been turned into a versatile tool to study structural properties of quantum dots which are essential for understanding their self-organised growth and quantum confinement effects. q 1998 Elsevier Science S.A. All rights reserved.

Keywords: X-ray scattering; Quantum dots; Semiconductor nanostructures; Self-assembled growth

1. Introduction

The fascinating opto-electronic properties of nanometer sized islands evolving during the so-called coherent Stranski–Krastanow growth in lattice mismatched semiconductor heterostructures has attracted world wide interest in recent years [1]. Although the novel quantum confinement effects are dependent on size, shape and strain of the islands the classical method as X-ray scattering to investigate these quantities, has hardly been applied to self-assembled islands on substrates. Using conventional large angle high resolution X-ray diffraction Darhuber [2] characterised strain distribution and correlations in the case of Ge islands embedded in a SiGe superlattice. However,

the scattering signal from the islands is so weak that it appears to be infeasible to use this method for a single layer of quantum dots on a substrate. Moreover, only information averaged over the whole multilayer stack can be obtained by large angle diffraction. In contrast, surface sensitive X-ray scattering, performed under grazing incidence and exit angles has been shown to be a valuable tool to study near surface structures of crystalline samples both structured vertically [3] and laterally [4]. Fig. 1 shows the basic scattering geometry. The incoming X-ray beam hits the sample surface at a grazing angle close to the critical angle for total external reflection, a_c. The scattered signal is collected under grazing exit angles a_f either in forward direction (grazing incidence small angle scattering (GISAXS)) or at large in-plane diffraction angles $2u$ (grazing incidence diffraction (GID)). The penetration- or information depth of the X-rays is controlled by a_i and a_f and is kept constant during a scattering experiment. For quantum dot structures

* Corresponding author. Fax: 149-892-1803182; e-mail: thmetzger@lrz.uni-muenchen.de.
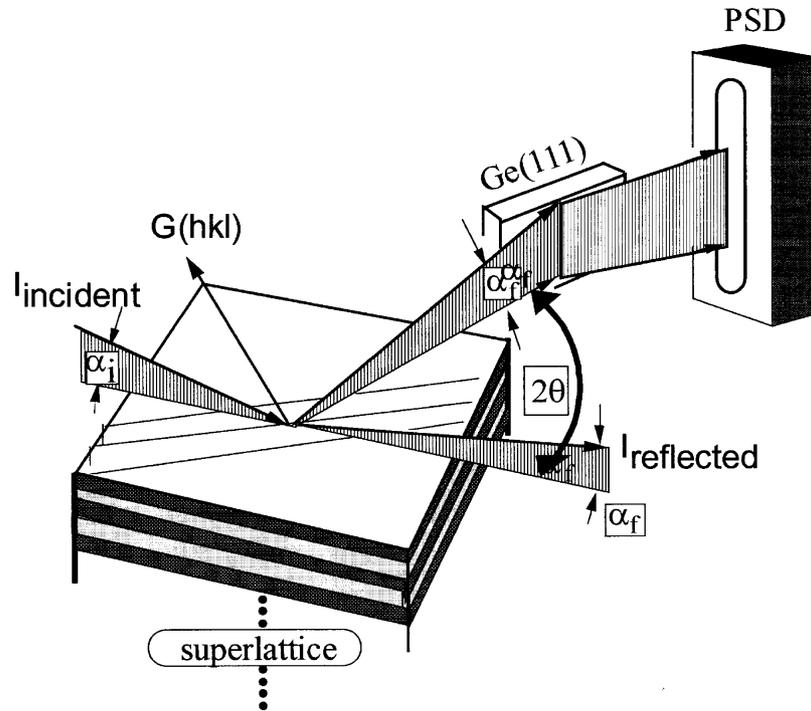[1] Present address: Dep. De Fisica-UFMG caixa nostal 702 Belo Horizonte MG, Brazil.

Fig. 1. Scattering geometry for high resolution grazing incidence small angle X-ray scattering (GISAXS) and diffraction (GID).
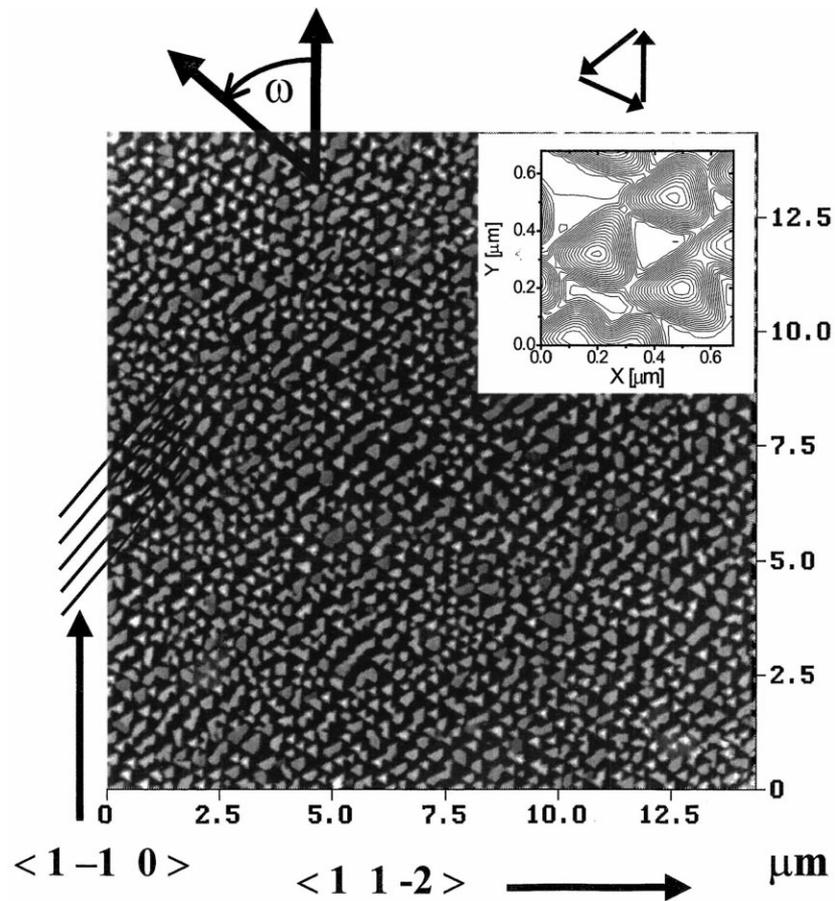

Fig. 2. Atomic force microscopy of Ge Islands on a Si(111) substrate. Notice the alignment of the islands (see lines). The inset shows their detailed triangular shape with the arrows pointing along the three different {110} directions.
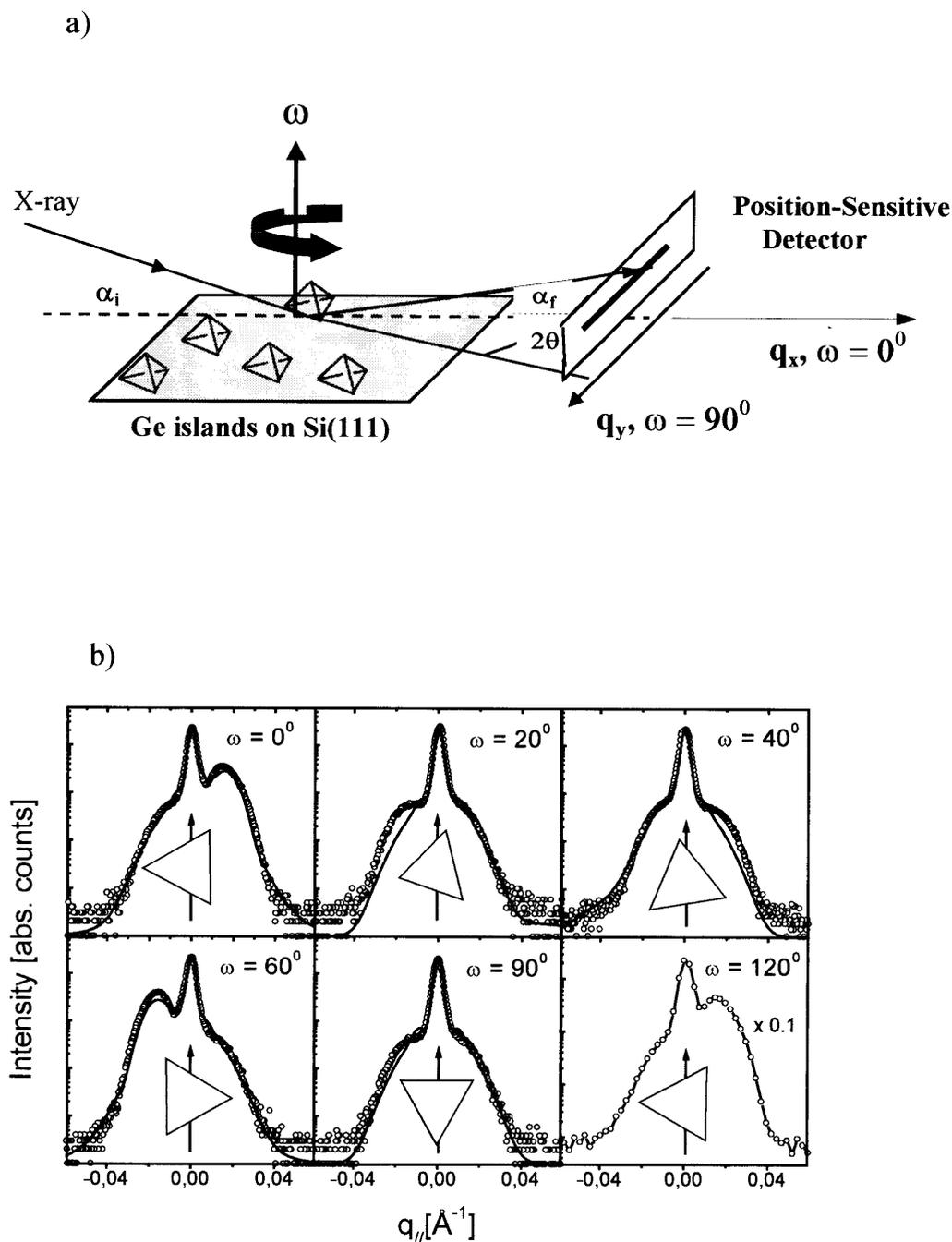
a)

b)

Fig. 3. (a) Geometry of GISAXS used to study the triangular Ge islands. (b) Scattering patterns for different ω. The triangles indicate the orientation of the islands with respect to the incident beam (arrows). The solid lines are least-squares fits (see text).

hundreds of nanometers by choosing appropriate grazing angles. At a selected depth sensitivity, the GISAXS signal contains information on the outer shape and size distribution of the quantum dots as well as on inter-dot correlations. Strain is most easily measured by diffraction (GID) at large in-plane angles 2θ (see Fig. 1). We have developed a novel technique which will be demonstrated in Section 3. By tuning in to a certain strain state we study the lateral diameter of the corresponding iso strain area by evaluating the small angle X-ray diffraction between the surface Bragg

peak of the substrate and the island material. Using this 'iso-strain scattering' technique we are able to quantify the inter-dependence of strain and lateral dimension of islands grown either coherently or relaxed on a substrate.

The paper is structured as follows: In Section 2 we report on results of boron induced growth of incoherent, relaxed Ge islands on Si(111). For coherent systems the corresponding results will be shown for InAs on GaAs(100) and Ge islands embedded in a Ge/Si superlattice in Sections 3 and 4, respectively.
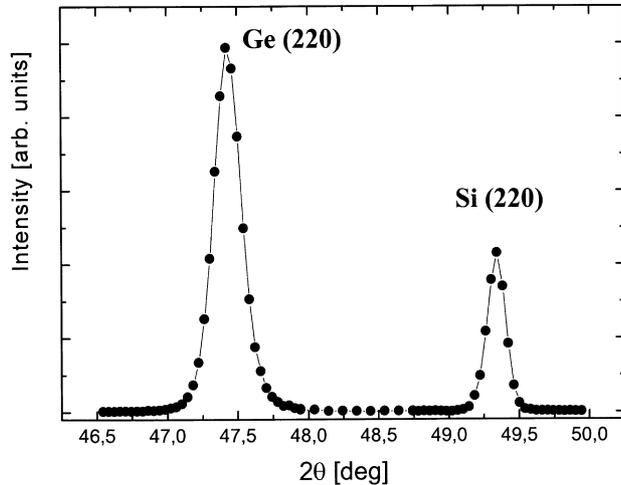
Fig. 4. (220) surface reflections of Ge islands and Si(111) substrate as a function of the scattering angle 2θ. The peaks appear at the positions for relaxed Ge and Si.

2. Relaxed Ge islands on Si(111)

The Ge/Si(111) sample, investigated by atomic force microscopy (AFM) and GISAXS, was prepared by molecular beam epitaxy in a UHV system. The substrate (kept at 530°C) was a Si(111) wafer with a ~0.45° miscut angle. A 1500 Å thick Si buffer layer was grown followed by 0.33 monolayers of boron (which exhibits a $\sqrt{3} \times \sqrt{3}$ reconstruction on Si(111)). Finally a 150 Å thick Ge layer was deposited at a rate of 0.25 Å/s. For Ge on Si with a lattice mismatch of 4%, the critical thickness for relaxation amounts to about three Ge monolayers. Thus, in the present case of 15 nm Ge, relaxation should occur resulting either in a highly defective but homogeneous Ge layer or in the growth of 3D islands. It was, a priori, not known whether such islands would be coherently strained or relaxed. In our analysis we find that, if boron is used as a surfactant, we obtain relaxed pyramidal islands, while growth on the uncovered 7×7 reconstructed pure Si(111) surface leads to a homogeneous relaxed Ge layer.

The inset of Fig. 2 shows the detailed shape and size of a few Ge islands, determined by AFM. They are pyramidal with well-defined {113} facets, base length $L \sim 2000$ Å and height $H \sim 300$ Å with some of them exhibiting a small (111) terrace of length $L_{top} \sim 100$ Å on top. The tendency for the islands to order can be seen in Fig. 2 indicated by the parallel lines. The islands are aligned in rows in the direction parallel to the terrace steps induced by the miscut. The degree of ordering was quantified from the height–height correlation function of the islands from Fig. 2. These results will be reported elsewhere (unpublished data).

We turn now to the GISAXS experiment performed at the X-ray beamline D4 at HASYLAB, DESY in Hamburg (Germany). As shown in Fig. 3a, the sample surface sees the well collimated primary beam at a grazing angle $\alpha_i = 0.24°$ (wavelength 1.77 Å). The scattering angle α_f was set

to 0.6° to collect only diffuse non-specular intensity, as described in Ref. [5]. The diffuse X-ray scattering from the islands was measured as a function of $|q_{//}| \approx (2\pi/\lambda) \sin 2\theta$ with a position-sensitive detector placed parallel to the sample surface. The scattering was measured for several azimuthal angles ω, corresponding to scans in different directions in the q_x–q_y plane. Fig. 3b shows selected scans in this scattering geometry, where the symmetry properties of the scattering patterns clearly appear: At $\omega = 0°$ the scattering intensity from the islands exhibits a shoulder on the right side of the central peak. This shoulder moves to the left after the sample has been turned to $\omega = 60°$, and returns to its original position for $\omega = 120°$. The patterns are symmetrical for $\omega = 30°$, 90°, 150°, and so on. The symmetry properties of these scattering patterns prove that the triangular symmetry of the islands can be determined using GISAXS as long as they are all oriented in the same direction. To reproduce the X-ray scattering patterns in detail we have calculated the scattering structure factor of triangular pyramids in GISAXS geometry in the Born approximation. Using the model structure factor squared we have fitted the first five patterns of Fig. 3b simultaneously, yielding $H = 190 \pm 10$ Å, $L = 1800 \pm 100$ Å, $L_{top} = 200 \pm 100$ Å and a Gaussian size distribution (FWHM = 50%). Since the AFM image and the symmetry properties of the GISAXS pattern indicate that the triangular pyramids all point in the same direction (perpendicular to the $\langle 1$-$10 \rangle$) no rotational dispersion was introduced in the calculation. Details will be given elsewhere (unpublished data).

The grazing-incidence geometry with $q_z \neq 0$ was essential to determine the triangular symmetry of the islands. If a similar q_x–q_y mapping was performed in transmission geometry with $q_z = 0$, the X-ray diffuse pattern would be symmetrical with respect to the origin of reciprocal space. As a result, a 6-fold pattern would be observed instead, corresponding to the projection of the pyramid on the base plane. The structure factors that have been calculated for $q_z = 0$ (conventional SAXS) and $q_z = 0.052$ Å^{-1}
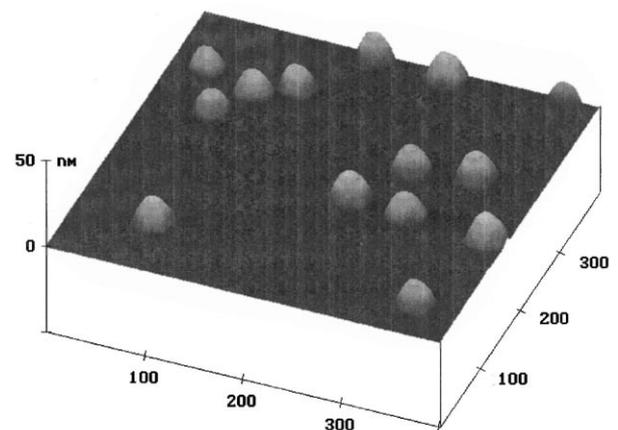

Fig. 5. Atomic force microscopy of InAs islands on GaAs(001) showing 'sugar-cone' like structures.

(GISAXS) showing the expected symmetries (unpublished data). In contrast to the GISAXS case, in SAXS experiments at $q_z = 0$ neither the shape nor the orientation of the triangular pyramids can be determined. We point out that this feature of GISAXS may be used to determine shape and symmetry of arbitrary structures, even if they are buried by cap layers.

Finally the (220) surface reflections of Ge on Si were investigated by GID measurements. As shown in Fig. 4 we find two Bragg peaks with the lattice parameter of Si and Ge, respectively. We conclude that the pyramids consist of pure Ge which is completely relaxed and incoherently connected with the Si substrate. In order to study the influence of boron on the Ge growth, we have also prepared samples with the same growth parameters except for the boron deposition. Using GISAXS, GID and specular reflectivity measurements we found clear evidence that in this case a homogeneous relaxed Ge layer (thickness 14.2 nm) has formed on the Si(111) surface and no islands are present (unpublished data).

3. 'Iso-strain scattering' from coherent InAs islands on GaAs(100)

InAs islands have been grown on GaAs(100) by MBE at 530°C substrate temperature and As partial pressure of 1×10^{-5} Torr. These growth parameters result in dislocation free InAs islands [6], which remain coherent although the lattice mismatch amounts to about 7% for this system. The surface of the samples was analysed by AFM after being exposed to air. Evaluation of the corresponding image (see Fig. 5) yields 'sugar-cone' like dots with heights of 100 ± 10 Å, dot diameters of 340 ± 60 Å and a Poisson-like lateral distribution with a mean distance of 500 Å, i.e. no lateral correlations are found at the low coverage of 10^9 dots/cm^2.

The X-ray measurements were performed at the BW2 beamline at HASYLAB/DESY with a wavelength of 2.07 Å. For GISAXS measurement the set-up as shown in Fig. 2a has been used, with $\alpha_i = 0.6°$ and $\alpha_f = \alpha_c = 0.4°$. The diffuse small angle scattering signal as a function of $q_\parallel$ is found to be independent of the azimuth angle ω as demonstrated in Fig. 6. From fits of the form factor for cylindrical dots, the average diameter is determined as 30 nm with a size dispersion of 50%. The latter is partially due to the conical shape of the dots.

Three-dimensional mapping of reciprocal space (RSM) in GID geometry has been performed by tracing angular scans at different radial positions between the (220) surface reflections of InAs and GaAs. The intensity distribution perpendicular to the sample surface, was simultaneously recorded by a position sensitive detector as shown in Fig. 1. The measurement was performed at an incidence angle α_i below the critical angle for total external reflection, which limits the penetration depth of the X-rays to about 10 nm, thus the scattering stems primarily from the InAs dots. The

footprint of the X-rays on the sample surface was about 1 mm^2 and ensured reliable sampling statistics. Fig. 7b shows an overview of the GID measurements. The height dependent strain in the islands leads to a variation of the lateral lattice parameter and, hence, to a spreading of the intensity distribution along the radial direction q_r from the position of the GaAs (220) at $q_r = 0$, to the position of the corresponding reflection of unstrained InAs, at $q_r = -0.225$ Å^{-1}. The finite extension of the islands results in a broadening in the q_a- and q_r-direction. We can show [7] that the q_a-broadening is solely due to the form factor of the islands and thus, a separation between strain and shape effects becomes possible. The meaning of radial and angular directions, q_r and q_a, respectively, is explained in Fig. 7a. We assume that the InAs islands are cylinders with a lattice parameter and perimeter depending only on the height in the dots. The strain distribution ranges from fully strained at the bottom of the dots to completely relaxed at their top. The strain distribution is then modelled by cylindrical disks with a constant lattice parameter and radius. These disks represent the 'iso-strain-areas', which give rise to the scattering intensity distribution in reciprocal space. The lateral dimension of the iso-strain-areas at the top of the dots is small and relaxed, thus yielding a broad intensity distribution along $q_{angular}$ at the largest possible deviation q_{radial} from the GaAs substrate peak. Close to the interface between the InAs dot and the GaAs substrate the iso-strain-area is large and completely strained to the lattice parameter of the substrate. Correspondingly we expect to find a sharper intensity profile along $q_{angular}$ at small q_{radial}. This qualitative picture is in agreement with our measurements as shown in Fig. 7b.
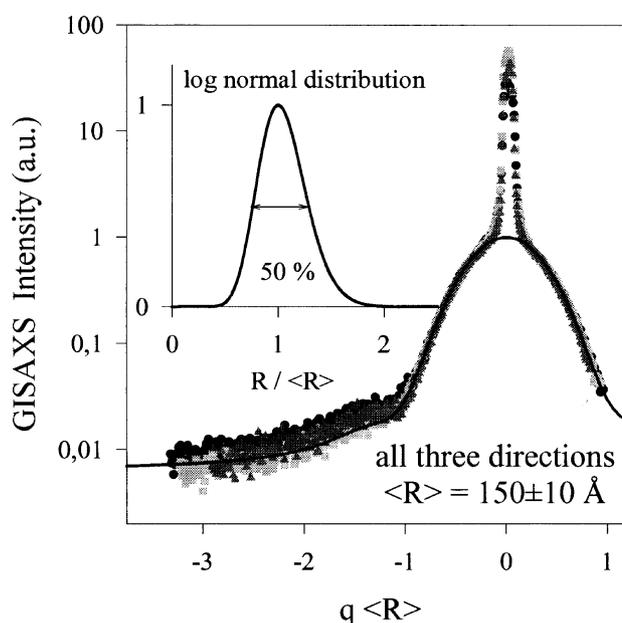

Fig. 6. GISAXS measurement from InAs islands on GaAs(001). The symbols represent three different azimuthal angles yielding the same scattering patterns. The solid line is a fit through the data points resulting in the average dot radius and the size dispersion (inset).
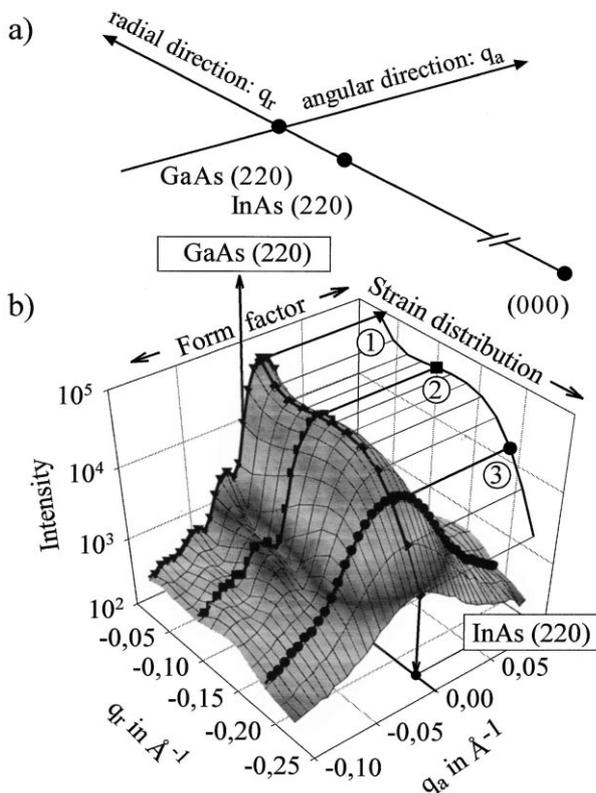
a)

Fig. 7. (a) Schematic view of the scan directions in reciprocal space close to the (220) GaAs and InAs surface Bragg reflections. (b) Dot induced intensity distribution between the GaAs and InAs (220) surface reflections. The strain dependent intensity change is projected onto the I–q_r plane. The dot form factor-induced intensity variation appears along the q_a-direction. The mesh represents all measured q_r–q_a scans.

The details of the quantitative analysis which yields the interdependence of strain and shape of the quantum dots will be given elsewhere [7]. The results are displayed in Fig. 8 where the radius of the iso-strain disks r and the gradient $g' = dg/dz$ of the reciprocal lattice parameter $g = 2\pi/a$, with respect to the height z, are plotted as functions of the relaxation. Fig. 8a shows that the interdependence of relaxation and radius r is linear except for the measurement closest to the GaAs reflection, where crossover effects from the transition of the dot into the substrate can no longer be neglected. The strain gradient g' as a function of relaxation $\delta a/a$ is shown in Fig. 8b. Again, the first data point should be omitted from further conclusions for reasons mentioned above. The local strain gradient first decreases and then increases with the lateral relaxation and becomes strongest at the top end of the dot where the InAs lattice can relax freely.

4. Coherent Ge dots embedded in a Si/Ge superlattice

It has been shown that Ge islands on Si(100) are usually rectangular pyramids, with {105} facets and can be grown with a narrow size distribution [8,9]. Since there are two

equivalent {100} directions in the plane of the substrate, it is difficult to minimise size and shape dispersion of these islands. Improvements of these distributions through self-organised island ordering has been achieved by the propagation of strain throughout the different layers of a SiGe superlattice. This self-organisation evolves after several Ge/Si bilayers are deposited.

The system Ge/Si with a lattice mismatch of 4% exhibits the coherent island growth mode. Information on self-organised ordering mechanisms relies crucially on a thorough investigation of lateral and vertical correlations evolving during growth of a superlattice. Surface sensitive GID is ideally suited for the correlation analysis of the Ge dots since its sensitivity can easily be tuned from the near surface region (about 10 nm) to a penetration of several hundreds of nanometers.

The present Ge/Si quantumdot superlattice was grown by MBE at a substrate temperature of 670°C on a (001) oriented Si wafer at a deposition rate of 0.075 Å/s and a nominal coverage of 5.5 monolayers of Ge. In order to improve on the lateral inter-dot correlation and the size uniformity, 19 bilayers containing the Ge dots and 400 Å Si were consecutively deposited on the substrate. The Ge content in the dots was estimated to be 70% [10]. The growth was terminated by the deposition of Ge thus leaving the surface with an
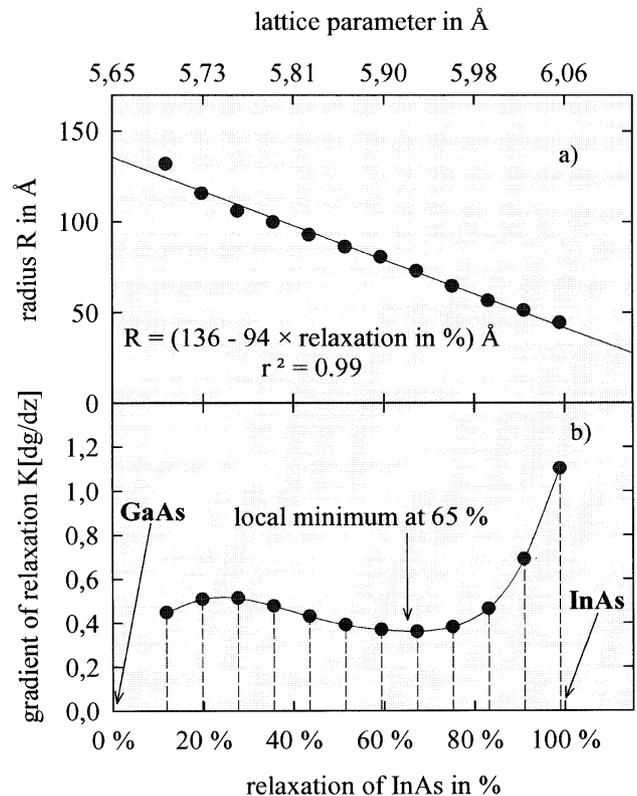

Fig. 8. (a) Dot radius r and (b) strain gradient $k\,dg/dz$ of the iso-strain areas as a function of strain relaxation in percent of the relative lattice mismatch $(a_{InAs} - a_{GaAs})/a_{GaAs}$. The straight line in (a) is a linear fit through the data. The curve in (b) represents a guide to the eyes.
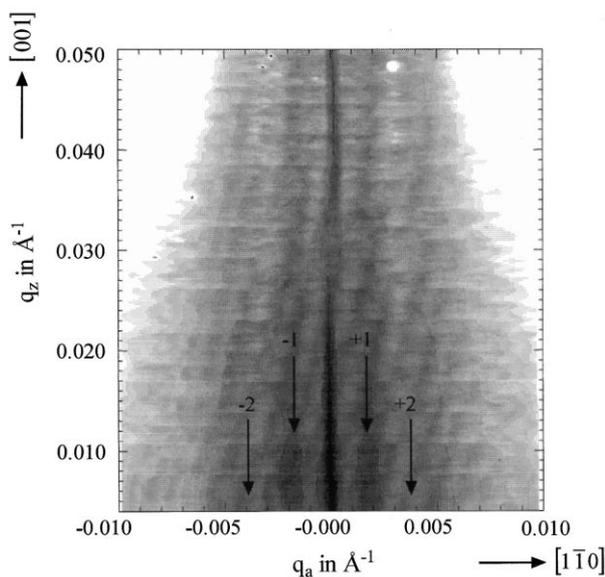
Fig. 9. Reciprocal space map in the q_a–q_z plane close to the (220) reflection of Si at the surface of a GeSi superlattice. The incident angle is $\alpha_i = 0.15°$ ($<\alpha_c$). The correlation maxima are indicated by ±1 and the shape induced intensity modulation by ±2, respectively. The central intensity rod at $q_a = 0$ is due to the Bragg peak of the substrate.

Fig. 11. Reciprocal space map in the q_a–q_z plane close to the (220) Si reflection for a GeSi superlattice with embedded Ge islands. The incident angle α_i is larger than α_c. Correlation induced intensity maxima are found along q_a and q_z showing that the buried dots are correlated in the growth direction.

uncovered array of Ge islands reflecting the lateral correlation developed during the multilayer growth.

GID measurements have been performed at the BW2 beamline at HASYLAB/DESY and at the TROIKA beamline at the ESRF. In both cases the in-plane resolution has been improved by the introduction of a Ge(111) analyser crystal between the sample and the PSD (see Fig. 1) result-
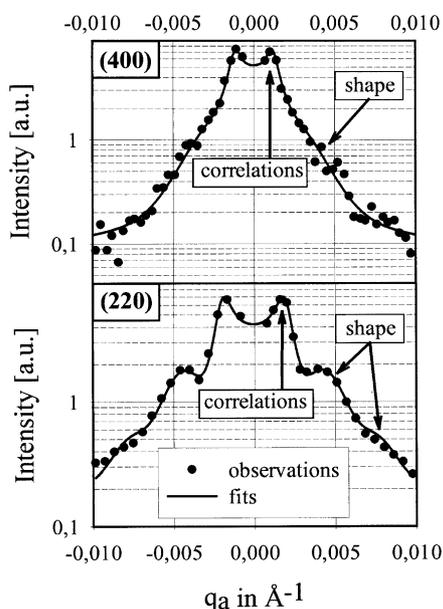

Fig. 10. Intensity distribution induced by Ge islands on a SiGe superlattice in the angular directions ⟨1-10⟩ and ⟨010⟩, close the (220) and (400) surface Bragg peaks, respectively. The fits show that the intensity modulations along q_a are due to correlation and shape effects (see text).
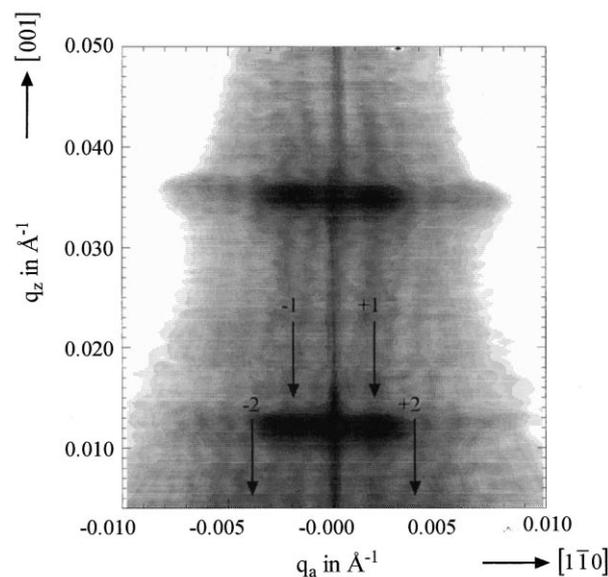
ing in a resolution of $\Delta q_{angular} = 0.0003$ Å^{-1}. The intensity distribution close to the (220) and (400) surface reflections of Si was mapped out in three dimensions at an incidence angle of $\alpha_i = 0.15°$ ($<\alpha_c$). Only the dots on the surface contributed to the scattering intensity because the penetration depth is much smaller than the thickness of the underlying Si spacer layer. From q_a versus q_r mappings we find the dots to be partially relaxed but coherently embedded in the Si layers (unpublished data). Here we turn our attention to the lateral and vertical correlation of the dots. Fig. 9 shows the q_a–q_z intensity mapping through the (220) reflection for $\alpha_i = 0.15°$. At $q_a = 0$ the surface reflection is elongated along q_z (so-called 'crystal truncation rod' scattering). In both directions the central rod is accompanied by two satellite rods, which are due to the inter-dot correlations. With a correlation analysis presented elsewhere [11] we can explain the intensity distribution along q_a at $q_z = 0$ as shown in Fig. 10. The fit in the lower panel of Fig. 10 indicates that the second maximum at $q_a = \pm 0.004$ Å^{-1} is due to the dot form factor while only the first maximum gives the correlation length $d_{110} = 2700$ Å in ⟨1-10⟩ direction. Fig. 10 upper panel shows the results of a similar analysis close to the (400) reflection in ⟨010⟩ direction, where the correlation length is larger by a factor of 1.48 ± 0.07. We conclude that the Ge dots are arranged in a short range order square lattice.

Finally the vertical dot correlation is investigated by increasing the penetration depth of the X-rays ($\alpha_i > \alpha_c$). The corresponding RSM in the q_z–q_a plane is shown in Fig. 11. The intensity distribution exhibits streaks along the angular direction at q_z values corresponding to the peri-

odicity of the superlattice (so-called 'diffuse Bragg sheets' [12]). These Bragg sheets are modulated at q_a positions specific for the lateral ordering of the dots. Thus we conclude that the buried dots, which possess the same periodicity as the superlattice, must be correlated through the multilayer stack in growth direction. A detailed investigation of the growth induced vertical and lateral dot correlation is in progress.

References

[1] MRS Bulletin, 23(2), February 1998.
[2] A.A. Darhuber, et-al., Phys. Rev. B 55 (1997) 15652.
[3] U. Pietsch, H. Metzger, S. Rugel, B. Jennichen, I.K. Robinson, J. Appl. Phys. 74 (1993) 2381.
[4] K. Paschke, et-al., Appl. Phys. Lett. 70 (1997) 1031.
[5] T. Salditt, T. H. Metzger, J. Peisl, Phys. Rev. Lett. 73 (1994) 2228.
[6] D. Leonard, K. Pond, P.M. Petroff, Phys. Rev. B 50 (1994) 11689.
[7] I. Kegel, et al. Proc. MRS Spring Meeting (1998) in press.
[8] Y.-W. Mo, D.E. Savage, B.S. Swartzentruber, M.G. Lagally, Phys. Rev. Lett. 65 (1990) 1020.
[9] A.J. Steinfort, et-al., Phys. Rev. Lett. 77 (1996) 2009.
[10] A.A. Williams, et-al., Phys. Rev. B 51 (1995) 5617.
[11] I. Kegel, et al. Appl. Phys. Lett. (1998) submitted.
[12] T. Salditt, T.H. Metzger, J. Peisl, Phys. Rev. Lett. 73 (1994) 2228.